The International Journal of Advanced Manufacturing Technology (2018) 97:939–952
https://doi.org/10.1007/s00170-018-1987-9

ORIGINAL ARTICLE

On-line estimation of the tool-chip interface temperature field during turning using a sequential inverse method

Shuwen Huang[1] · Bo Tao[1] · Jindang Li[1] · Yajun Fan[1] · Zhouping Yin[1]

Received: 23 October 2017 / Accepted: 2 April 2018 / Published online: 15 April 2018

Abstract
It is well known that the direct measurement of temperature distribution at the tool-chip interface in a machining process is difficult to accomplish. Thus, this paper provides an on-line inverse technique to estimate the temperature field at the tool-chip interface of a turning tool, using temperatures measured at some sensor-accessible locations. A sequential Tikhonov regularization method (STRM) is proposed to determine the transient heat flux imposed at the tool-chip interface, by solving an inverse heat conduction problem (IHCP). Then, the temperature field at the tool-chip interface is computed by solving the three-dimensional non-linear thermal model, with a method combining Duhamel's superposition theorem with the finite element method. The procedure proposed shows a superiority in on-line applications due to its high computational efficiency and independence of future measurements. A comparison of the STRM with several other inverse methods in the literature was made through numerical tests. Experimental cutting tests on Ti-6Al-4V titanium alloy were done to validate the thermal model and method. Both numerical and experimental tests show that the proposed method can provide an efficient and easy-to-implement strategy for on-line temperature field monitoring of machine tools.

Keywords Inverse heat conduction problem · On-line tool state monitoring · Sequential Tikhonov regularization · Tool-chip interface temperature

Nomenclature

J	Functional
q	Heat flux (W/m^2)
T	Temperature (°C)
T_0	Initial temperature (°C)
T_∞	Ambient temperature (°C)
Y	Measured temperature (°C)
S	Boundary surface
k	Thermal conductivity (W/m°C)
c	Specific heat capacity (J/kg°C)
ρ	Density (kg/m^3)
h	Convective heat transfer coefficient (W/m^2°C)
t	Time coordinate (s)
t_f	Final time (s)
k	Time step index
x, y, z	Space coordinate (m)
i	Spatial index
M	Number of sensors
m	Sensor index
r	Number of future measurements
f	Feed rate (mm/rev)
v_c	Cutting speed (m/min)
a_p	Depth of cut (mm)
σ	Standard deviation
α	Regularization parameter
φ	Unit step temperature response
$\Delta\varphi$	Sensitivity coefficients

1 Introduction

On-line temperature monitoring of cutting tools during metal cutting process has been of interest for a long period because it helps to increase tool's lifetime, reduce products cost, and improve part quality. In machining processes, the energy caused by friction and plastic deformation is mainly converted into heat which dissipates into the newly deformed chip, the

✉ Bo Tao
taobo@mail.hust.edu.cn

[1] State Key Laboratory of Digital Manufacturing Equipment and Technology, Huazhong University of Science and Technology, Wuhan 430074, Hubei, People's Republic of China

workpiece, and the cutting tool. Basically, three regions of heat generation can be distinguished: the primary deformation zone, the tool-chip interface, and the tool-workpiece interface. Temperature rise in the tool is the combined effects of these heat sources and is determined by the distribution of heat flux at the contact area of the tool. The tool-workpiece interface heat source can be neglected if a sharp tool is used [1]. The heat conducting into the tool converges into the small tool-chip interface region, leading to a high local temperature field and a large temperature gradient in this region, which significantly affects the tool wear, workpiece surface quality, and chip formation mechanics. Therefore, there is an increasing demand to measure this tool-chip interface temperature field precisely and on-line.

As one of the most difficult tasks in metal cutting operations, temperature field measurement or estimation of cutting tools draws substantial attentions from researchers. Many experimental methods have been introduced to measure tool temperatures directly, such as the embedded thermocouple [2], tool-work thermocouple [3, 4], infrared imaging [5, 6], and thin film sensors [7]. A review of these direct measurement methods can be found in [8]. However, only average temperature or temperature field distant from the tool-chip interface can be obtained, because of the difficulties caused by the movement of the workpiece, the chip obstacles, and the small contact area.

Many theoretical methods, including two-dimensional analytical treatments [9, 10] and numerical methods, such as the finite difference method [1], the finite element method [11, 12], and the boundary element method [13] have been developed to calculate or simulate the tool-chip interface temperature field. Zhang et al. [10] developed an analytical model to investigate coated cutting tool rake face temperature distribution, where an explicit rake face temperature prediction model was successfully applied. However, the analytical models are usually based on many simplifying assumptions, which affect the accuracy of calculation for complex tool geometry and non-linear models. The numerical simulations [1, 11–13] are rarely applied in on-line applications because of the low computational efficiency. Furthermore, boundary conditions of the thermal model are usually not known precisely, such as the heat flux flowing into the tool-chip interface.

In recent years, the studies of inverse heat conduction problem (IHCP) have offered convenient alternatives to obtain accurate heat flow or temperature distribution in machining processes. Generally, estimating the heat flux flowing into the cutting tool using temperatures measured at some sensor-accessible locations is called an "inverse heat conduction problem (IHCP)," while computing the temperature field by solving the thermal model with the already known heat flux is called a "direct heat conduction problem (DHCP)." The IHCP is a mathematically "ill-posed" problem, which is extremely sensitive to measurement errors, and the main challenge of the IHCP is how to stabilize or regularize the result [14].

Yen et al. [15] firstly developed an inverse estimation scheme based on an analytical one-dimensional elliptical model and their model is relatively simple with well-defined tool geometry and boundary conditions. Similar works were carried out by Stephenson [16] and Kwon et al. [17]. Lavisse et al. [18] determined grinding heat flux distribution successfully by using the inverse heat transfer method based on the steady-state temperature distribution expression. In these analytical inverse works [15–18], the thermal model geometry and boundary conditions have been simplified to some extent, which are generally thought to be inappropriate to describe the real heat conduction in machining, especially when the thermal model's non-linearity and irregular shape of the tool-chip contact boundary are considered.

Iterative regularization methods have been applied for complex three-dimensional thermal models [19–22]. Carvalho et al. [19] developed a three-dimensional inverse algorithm in transient conditions for heat flux and cutting temperature estimation. The direct problem was solved numerically by the finite volume method while the inverse problem was solved using the golden section technique. Huang et al. [20] applied the steepest descent method in determining the surface heat fluxes on the cutting edges of cutting tools. Liang et al. [21] utilized a three-dimensional inverse heat conduction procedure based on the golden section technique to investigate the quantitative tool-chip interface temperature of the heat pipe cutter. Liang et al. further their study in [22] to determine the steady-state tool-chip interface temperature in dry turning based on the conjugate gradient method. The estimation accuracy has been significantly improved by these iterative inverse methods; however, low computational efficiency still limits their application in on-line requirements.

More recently, several intelligent algorithms are also used to solve IHCP in machining. Wei et al. [23] established a dynamic temperature field model of solid cemented carbide milling cutter and an inverse solution based on the particle swarm optimization algorithm to solve the heat flux in power series form. Similarly, the particle swarm optimization algorithm was used in [24] to identify the heat flux in the tool-workpiece interface during milling.

As a "near real-time" inverse method, the sequential function specification method (SFSM) is firstly proposed by Beck [14] using the so-called future time regularization to estimate and stabilize the current heat flux component. Norouzifard et al. [25] utilized the SFSM to estimate the heat flux entering the cutting tool, and thermocouples inserted into specific locations of the cutting tool provide the inverse solver input data. The temperature distribution in the tool was computed by performing transient thermal

analysis using a three-dimensional finite element model. Similarly, Brito et al. [26], Chen et al. [27], and Samadi et al. [28] employed the SFSM to estimate heat fluxes at the rake face of cutting tools, and Battaglia et al. [29] applied the SFSM in heat flux estimation in high speed drilling.

Though a substantial number of researches have been done, there still exist two limitations of the existing inverse methods. On the one hand, time delay exists in most of the methods since future measurements, several time steps for the SFSM, and whole-time steps for the iterative methods are required to estimate the current heat flux component. On the other hand, the computation strategy of three-dimensional and non-linear thermal model cannot satisfy the requirement of on-line calculation.

To overcome these limitations, an on-line inverse method is proposed to estimate the time-dependent heat flux and temperature field at the tool-chip interface of a turning tool. The sequential Tikhonov regularization method (STRM) is proposed to estimate the heat flux component sequentially without using any future measurement data. To improve the calculation efficiency of the thermal model, Duhamel's superposition theorem is combined with the finite element method. The procedure proposed is suitable for on-line applications due to its sequential nature and high computational efficiency. Both numerical and experimental tests were carried out to validate the accuracy and efficiency of the proposed method.

2 Thermal model of the turning tool

A practical turning tool and the corresponding thermal problem scheme with boundary conditions are shown in Fig. 1. An uncoated carbide insert with a rake angle of 7° and a relief angle of 7° was used as cutting tool.

In turning process, the heat conducts into the tool mainly through the tool-chip interface and the tool-workpiece interface, and the tool temperature field is determined by the heat flux distribution at these two interfaces. In this study, only heat flux at the tool-chip interface on the rake face is considered since the heat generated at the tool-workpiece interface can be neglected because of the tool insert's positive relief angle [1]. What is more, the tool-chip interface is very small so that the heat flux is reasonably considered to be uniformly distributed [20].

The tool-chip interface is denoted as S_1 in Fig. 1 and is subject to an unknown time-dependent heat flux, $q(t)$. The surfaces between the shim, insert, and tool holder are denoted as S_2 and the remaining surfaces exposed to the ambient air are denoted as S_3. The tool receives the surface heat flux $q(t)$ and is cooled by convection with the environment during turning process.

The governing equation of this three-dimensional transient heat conduction problem can be expressed as

$$\frac{\partial}{\partial x}\left(k(T)\frac{\partial T}{\partial x}\right)+\frac{\partial}{\partial y}\left(k(T)\frac{\partial T}{\partial y}\right)+\frac{\partial}{\partial z}\left(k(T)\frac{\partial T}{\partial z}\right) = \rho c(T)\frac{\partial T}{\partial t} \quad (x,y,z)\in\Omega, t>0 \tag{1}$$

where $T(x, y, z, t)$ is the temperature; ρ is the mass density; and $c(T)$ and $k(T)$ are the temperature-dependent specific heat and thermal conductivity, which make the problem a non-linear one.

The boundary conditions are

$$-k(T)\frac{\partial T}{\partial \eta} = q(t); \qquad (x,y,z)\in S_1, t>0 \tag{2}$$

$$-k(T)\frac{\partial T}{\partial \eta} = h_{c1}(T-T_\infty) \qquad (x,y,z)\in S_2, t>0 \tag{3}$$

$$-k(T)\frac{\partial T}{\partial \eta} = h_{c2}(T-T_\infty) \qquad (x,y,z)\in S_3, t>0 \tag{4}$$

$$-k(T)\frac{\partial T}{\partial \eta} = h_{c}(T-T_\infty) \qquad (x,y,z)\in S_4, t>0 \tag{5}$$

Equation 2 is the boundary condition of the tool-chip interface (S_1), where $\partial T/\partial \eta$ is the derivative along the outward drawn normal to the subject surface, and $q(t)$ is the time-varying heat flux.

Equations 3 and 4 are the boundary conditions of the contact areas between the tool holder and tool fixture (S_2) and between the tool insert and tool holder (S_3), respectively. h_{c1} and h_{c2} are the corresponding thermal contact conductance. T_∞ is the ambient temperature which is predefined as 20°C in this study. Equation 5 is the boundary condition of the remaining area exposed to the ambient air (S_4), and h_c is the convective heat transfer coefficient between the tool and ambient air.

The thermal contact boundary conditions described by Eqs. 3 and 4 are simulated by considering a 10 μm air gap with air property of 50 and 30°C, respectively, as recommended in [19].

The initial condition is

$$T(x,y,z,0) = T_0 \tag{6}$$

The thermo-physical parameters of the materials used in the thermal model are listed in Tables 1 and 2. The tool insert is an ISO K10 grade uncoated carbide and the tool fixture, tool holder, and shim are manufactured from AISI 1045 steel.

During a practical turning process, $q(t)$ is unknown, and the task of the inverse technique is to determine this time-varying heat flux using the knowledge of temperatures measured by temperature sensors. If all material properties and boundary conditions, including $q(t)$, are

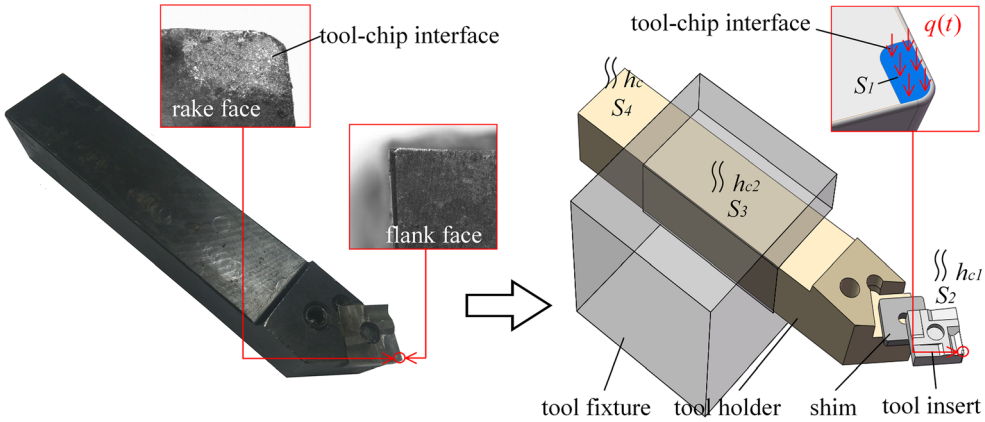

Fig. 1 A practical turning tool and the thermal model with boundary conditions

known precisely, Eqs. 1, 2, 3, 4, 5, and 6 represent the direct heat conduction problem, and the task of such a problem is to solve these equations and obtain the temperature field. For an on-line application, the computation of the direct problem must be with high efficiency.

3 The direct problem

Numerical methods such as the finite element method (FEM) and the boundary element method (BEM) can be applied to solve the thermal model. However, low computational efficiency limits the application of these methods in on-line applications. In this paper, a method combining Duhamel's theorem and the finite element method is proposed to solve the non-linear thermal model with high efficiency.

3.1 Duhamel's theorem

Duhamel's theorem is based on the superposition principle. If any known heat flux, $q(t)$, is applied, the corresponding temperature field for any region can be calculated by Duhamel's superposition integral:

$$T(x,y,z,t) = T_0(x,y,z,t) - \int_0^t q(\lambda)\frac{\partial\varphi(x,y,z,t-\lambda)}{\partial\lambda}d\lambda \qquad (7)$$

Table 1 Thermo-physical parameters of the materials

	Thermal conductivity (W/m$^{2\circ}$C)	Density (kg/m^3)	Specific heat capacity (J/kg$^\circ$C)
Cemented carbide	(Table 2)	14,830	(Table 2)
AISI 1045	45	7800	473
Air at 20 °C	0.025	1.164	1013
Air at 30 °C	0.027	1.056	1017
Air at 50 °C	0.034	0.789	1030

The discrete form can be written as

$$T_{i,k} = T_{i,0} + \sum_{n=1}^{k} q_n \Delta\varphi_{i,k-n} \qquad (8)$$

where subscript i is the spatial index denoting a location (x_i, y_i, z_i) where the temperature is to be calculated, and subscript k is the time index denoting time $(k-1)\Delta t \le t_k < k\Delta t$, while the time domain is discretized in equal time intervals Δt, $2\Delta t$, …, $k\Delta t$, … with a fixed Δt. $T_{i,0}$ is the initial temperature. $\Delta\varphi$ is the impulse temperature response or the so-called sensitivity coefficient, which is defined as

$$\Delta\varphi_{i,k-n} = \frac{\partial T_{i,k}}{\partial q_n} \qquad (9)$$

The sensitivity coefficient $\Delta\varphi_{i,k-n}$ denotes the temperature variation at location (x_i, y_i, z_i) and time t_k, due to an impulse change of heat flux at time t_n.

In practice, this sensitivity coefficient can be obtained by [14]:

$$\Delta\varphi_{i,k} = \varphi_{i,k+1} - \varphi_{i,k} \qquad (10)$$

where $\varphi_{i,k}$ is the temperature rise at t_k caused by a unit step heat flux input imposing constantly from the initial time, namely, by making $q(t) = 1$ in Eq. 2.

Duhamel's theorem implies that the temperature rise at time t_k is the integration of temperature variation caused by all heat flux component from time t_1 to t_k.

$\Delta\boldsymbol{\varphi_i} = [\Delta\varphi_{i,1}, \Delta\varphi_{i,2}, \Delta\varphi_{i,3}, \ldots]$ is used to denote the sensitivity coefficients from t_1 to the end of experiment. For a linear case, $\Delta\boldsymbol{\varphi_i}$ keeps unchanged at different time steps due to its independence of temperature variation. However, for a non-linear case, $\Delta\boldsymbol{\varphi_i}$ is dependent of temperature and may be different at different time steps because of the variation of the temperature field. In this case, Duhamel's superposition integral should be written as

$$T_{i,k} = T_{i,0} + \sum_{n=1}^{k} q_n \Delta\varphi_{i,k-n}^{k} \qquad (11)$$

$$\Delta\varphi_{i,k-n}^{k} = \varphi_{i,k-n+1}^{k} - \varphi_{i,k-n}^{k} \qquad (12)$$

Table 2 Temperature-dependent thermal conductivity and specific heat capacity of the insert [30]

Temperature (°C)	20	100	300	500	700	900
Thermal conductivity (W/m^{2}°C)	110	105	98	90	82	75
Specific heat capacity (J/kg°C)	220	244	290	320	328	337

where the superscript k denotes the kth time step and $\Delta\varphi_i^k$ is the sensitivity coefficients at the kth time step.

To compute the temperature variation with time, $T_{i,\ k}$ $(k = 1, 2, \ldots)$, the sensitivity coefficients $\Delta\varphi_i^k$ should be recalculated at each time step whenever the temperature field of the tool has changed, which is very time-consuming considering the complex geometry of the turning tool model.

3.2 Sensitivity coefficients computed by FEM

Obviously, the computation of the sensitivity coefficients in Eq. 11 has a controlling impact on the efficiency and accuracy of this method. The definition of Eq. 12 allows us to apply numerical techniques such as FEM to compute these coefficients. However, directly using the FEM computation in the on-line procedure could be time-consuming. Thus, in this paper, an off-line database which contains sensitivity coefficients occurring at different tool temperature fields is set up by using the commercial FEM software ANSYS, and then the appropriate sensitivity coefficients $\Delta\varphi_i^k$ for different time step k are selected from this database in the on-line procedure.

The flow chart illustrated in Fig. 2 shows how the overall procedure is executed.

The sensitivity coefficient database is obtained in the off-line stage, which can be summarized as follows:

Step 1. Simulate tool temperature fields in ANSYS by applying constant heat fluxes, $q(t) = c_j$, $(j = 1, 2, \ldots, J)$, at the tool-chip interface until the steady-state, where c_j is a constant value.

Step 2. Record the temperatures at the sensor locations, $T_m(c_j)$, $(j = 1, 2, \ldots, J)$, where the subscript m denotes the sensor location.

Step 3. Obtain the sensitivity coefficients $\varphi_i(c_j)$, $(j = 1, 2, \ldots, J)$ by adding a unit step to the original heat flux as $q(t) = c_j + 1$ in ANSYS, recording the unit temperature rise $\varphi_i(c_j)$, and substituting $\varphi_i(c_j)$ into Eq. 10.

The number of sensitivity coefficients in the database J depends on the degree of the thermal model's non-linearity. Generally, the more sensitivity coefficients are obtained, the more accurately can the temperature computation be. In this paper, 20 constant heat flux inputs were designed as $q(t) = c_j = j \times 10^6 W/m^2$, $(j = 1, 2, \ldots, 20)$. The maximum temperature of the 20 simulated temperature fields ranges from 100 to 1300 °C, which generally covers the temperature during the practical turning process.

Figure 3a shows the meshed tool model in ANSYS, where a total number of about 250 million elements are used. The material physical parameters (Tables 1 and 2), boundary conditions, and tool geometry of the FEM model are given in Section 2.

Figure 3b shows examples of the simulated tool temperature fields and the corresponding sensitivity coefficients obtained for a point (marked as i_1) at the tool-chip interface, by applying $q(t) = c_5 = 5 \times 10^6$W/m^2 and $q(t) = c_{15} = 15 \times 10^6$W/m^2, respectively.

The on-line computation stage can be illustrated as follows:

Suppose that the heat flux components $(q_1, q_2, \ldots, q_k)$ are available at time step k.

Step 1. Read the measured temperature at the sensor locations Y_m.

Step 2. Select the optimal j from $(1, 2, \ldots, 20)$ where the difference between Y_m and $T_m(c_j)$ is the smallest in all 20 sets.

Step 3. Set $\Delta\varphi_i^k = \Delta\varphi_i(c_j)$.

Step 4. Compute the temperature by substituting $\Delta\varphi_i^k$ and $q_n(n = 1, 2, \ldots, k)$ into Eq. 11.

Increasing k to $k + 1$ and repeat steps 1–4 sequentially, the temperature variation at location (x_i, y_i, z_i) can be computed on-line by the above procedure. If temperatures of hundreds of points at the tool-chip interface are obtained, the temperature field then can be reconstructed by interpolating these temperatures. In this study, 150 temperature points, whose computation time is within 0.5 s, are sufficient to reconstruct the temperature field of the tool-chip interface.

4 Heat flux estimation by the STRM

4.1 Mathematical fundamental of the STRM

To compute the temperature field on-line, the heat flux must be estimated in a sequential manner. The idea to solve an inverse problem is to formulate an optimization problem which minimizes the differences between the measured temperatures and the temperatures calculated from the direct problem solver at the sensor locations. The heat flux then can be estimated by minimizing the following least square form function:

$$J(q(t)) = \int_{t=0}^{t_f} \sum_{m=1}^{M} [T_m(t, q(t)) - Y_m(t)]^2 dt \quad (13)$$

where $q(t)$ is the heat flux function to be estimated, and $Y_m(t)$ are measured temperatures at sensor locations (x_m, y_m, z_m). M denotes the number of sensors. $T_m(t, q(t))$ is computed by the direct problem solver with an estimated $q(t)$. t_f is the final time of the measurement.

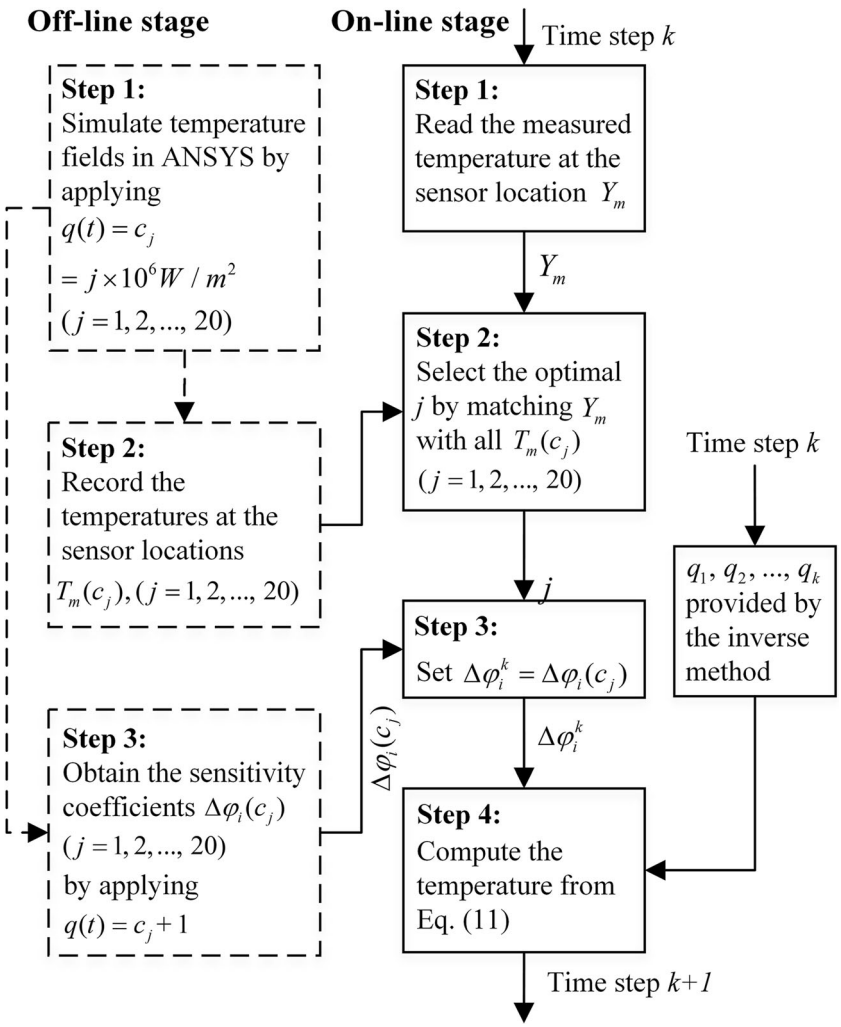

Fig. 2 Flow chart of the temperature computation procedure

To estimate the heat flux in real time, the least square function should be numerically discretized and transformed into a sequential manner. This idea is firstly proposed by Stoltz and adopted in the well-known sequential function specification method (SFSM) [14]. The piecewise-constant heat flux components ($q_1, q_2, \ldots, q_k, \ldots$) are used to represent $q(t)$. Then, the problem can be changed into a sequential optimization problem as:

$$J(q_k) = \sum_{m=1}^{M} \left[T_{m,k}(q_k) - Y_{m,k}\right]^2 \quad (14)$$

where the subscript k is the time index, and q_k is the heat flux component to be estimated at t_k. It is assumed that the previous heat flux components ($q_1, q_2, \ldots, q_{k-1}$) were already estimated.

An important characteristic of this form is its sequential nature: q_k depends only on the current temperature measurement $Y_{m,\,k}$, and k is increased by one at each time step sequentially.

The result of Eq. 14 is called an "exact matching" because the calculated temperatures $T_{m,\,k}$ are made as close as possible to the measured values $Y_{m,\,k}$. However, this result is usually unstable due to the problem's ill-posedness: small errors in the measurements, which is inevitable in a practical process, will lead to large fluctuations in the estimated results.

To stabilize this ill-posed problem, the Tikhonov regularization can be used by penalizing undesirable variation and reduce excursions in the unknown heat flux [31]. However, the conventional Tikhonov regularization is a whole-domain method in nature and cannot be applied in a sequential problem.

In this paper, a sequential Tikhonov regularization method (STRM) is proposed by adding a novel sequential Tikhonov regularization term to Eq. 14:

$$J(q_k) = \sum_{m=1}^{M} \left[T_{m,k}(q_k) - Y_{m,k}\right]^2 + \alpha\Omega(q_k, q_{k-1}, q_{k-2}) \quad (15)$$

where

$$\alpha\Omega(q_k, q_{k-1}, q_{k-2}) = \alpha_0 q_k^2 + \alpha_1 (q_k - q_{k-1})^2 + \alpha_2 (q_k - 2q_{k-1} + q_{k-2})^2 \quad (16)$$

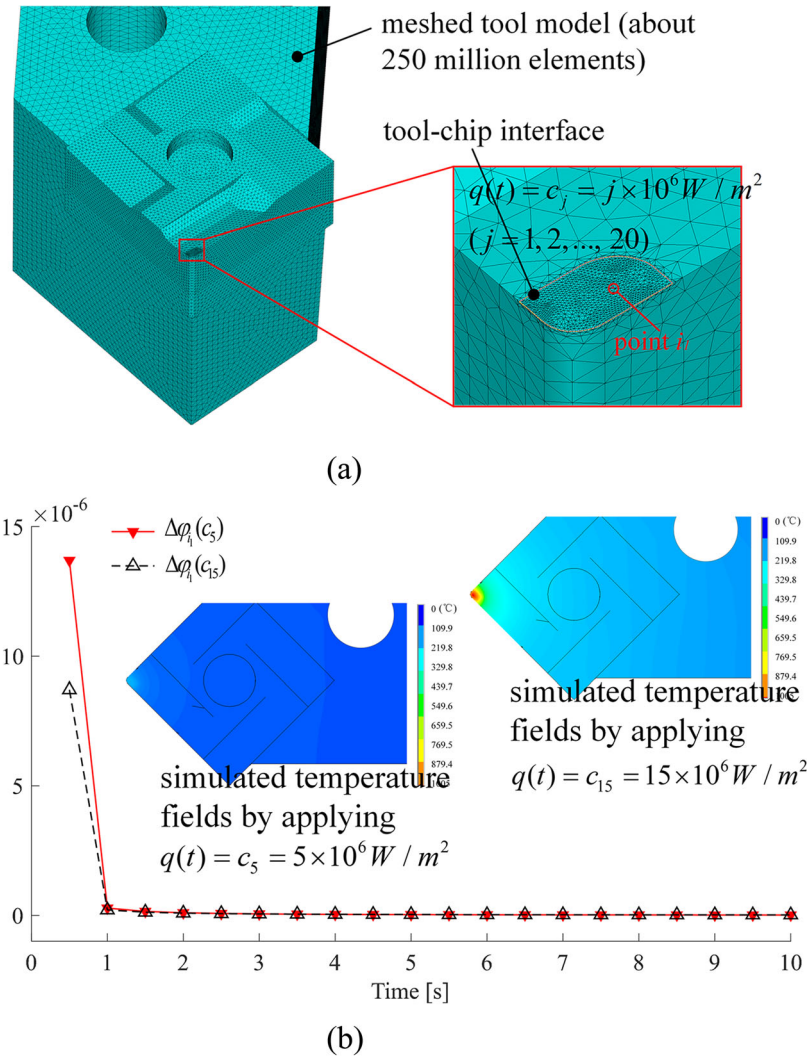

Fig. 3 **a** The meshed tool model in ANSYS and **b** an example of two simulated tool temperature field in ANSYS by applying $q(t) = c_5 = 5 \times 10^6 W/m^2$ and $q(t) = c_{15} = 15 \times 10^6 W/m^2$ and the corresponding sensitivity coefficients curve of point i_1

where $\alpha\Omega(q_k, q_{k-1}, q_{k-2})$ is called the regularization term, and α is the regularization parameter. $\alpha_0 q_k^2$, $\alpha_1(q_k - q_{k-1})^2$, and $\alpha_2(q_k - 2q_{k-1} + q_{k-2})^2$ are called zeroth-order, first-order, and second-order regularization terms, respectively, according to the order of derivative that is penalized.

Different from the well-known whole-domain Tikhonov regularization method and the SFSM, where time delay exists because extra future measurements are required to estimate the current component, the idea in STRM is to make use of the previous heat flux components' information with the help of the modified regularization terms. The effect of the regularization term is to reduce the magnitude of q_k and the magnitude of changes from q_k to its neighboring components and avoid extremely large components and rapid oscillations in the estimation.

By carefully choosing the regularization parameters $(\alpha_0, \alpha_1, \alpha_2)$, a balance between the effect of smoothing the estimation and minimizing the estimation error is made.

Substituting the expression of $T_{m,k}(q_k)$ (Eq. 11) into Eq. 15 and following the usual minimization of $J(q_k)$ with respect to q_k yield the inverse estimator:

$$q_k = \frac{\left(Y_{m,k} - \hat{T}_{m,k}\big|_{q_k=0}\right)\Delta\varphi_{m,0}^k + (\alpha_0 + 2\alpha_1)q_{k-1} - \alpha_1 q_{k-2}}{\sum_{m=1}^{M}\left(\Delta\varphi_{m,0}^k\right)^2 + \alpha_0 + \alpha_1 + \alpha_2} \tag{17}$$

where $\hat{T}_{m,k}\big|_{q_k=0}$ is the temperature rise calculated with the assumption of q_k=0, and $\Delta\varphi_{m,0}^k$ is the first element of the sensitivity coefficients.

Note that in Eq. 17, the calculation of q_k depends on the previous heat flux components $(q_1, q_2, \ldots, q_{k-1})$; the sensitivity coefficients, which is obtained from the off-line database; the current temperature measurements; and the pre-defined regularization parameters $(\alpha_0, \alpha_1, \alpha_2)$, which are obtained by a simple grid-search approach. All parameters needed to

compute q_k are known and can be provided in a sequential manner without using any future information. This characteristic makes the STRM suitable for on-line heat flux identification problem.

4.2 Numerical verification of the STRM

Numerical tests were carried out to verify the accuracy, stability, and robustness of the proposed STRM. Temperatures calculated by the direct solver using an assumed exact heat flux were used as inputs to the inverse procedure, and then comparison between the estimated heat flux and the exact one was made.

The estimation error is defined as the root mean square (RMS) error and relative root mean square (RRMS) error between the exact and estimated heat flux:

$$e_{\mathrm{RMS}} = \sqrt{\sum_{i=1}^{k} (\hat{q}_i - q_i)^2 / k} \tag{18}$$

$$e_{\mathrm{RRMS}} = 100\% \times e_{\mathrm{RMS}} / q_{max} \tag{19}$$

where q_i and $\hat{q}_i$ are the exact and estimated heat flux, respectively.

For comparison study, the heat flux is calculated by three different inverse methods, i.e., the exact matching method (result of Eq. 14), the SFSM, and the proposed STRM, respectively.

Five numerical tests, whose test conditions and estimation errors are given in Table 3, were carried out, all utilizing a step heat flux to simulate a rapidly changing cutting condition.

Gaussian noise with zero mean and deviation of $\sigma = 5$ °C (about 6% of the maximum temperature) or $\sigma = 10$ °C (about 12% of the maximum temperature) is added to the temperatures to simulate real cutting temperatures. The measurement interval is 0.5 s for all tests.

Figure 4 shows the estimation results for numerical test 1. The RRMS error is 15.2% for the exact matching method, 3.1% for the SFSM, and 3.2% for the STRM.

Figure 4a shows that the heat flux estimated by the exact matching method has rather violent fluctuations. The reason is that no additional information is utilized to regularize the problem, thus making the estimation extremely sensitive to measurement errors.

Figure 4b shows that the SFSM result has several seconds of delay compared with the assumed exact curves. The reason is that four steps of future measurements are used in this case. It can be seen from Table 1 that more future measurements are required when larger noise and further sensors are used.

Figure 4c shows that the estimation result of STRM is stable and with nearly no time delay since no future temperatures are used. There is a small fluctuation at the beginning of the curve, because no or only a few prior heat flux components can be used at the beginning. However, the estimation becomes rather stable as the time goes on.

It can be concluded from these comparisons that the proposed STRM is as stable as the SFSM and indicates a superior property in on-line applications as there is no or little time delay.

The numerical tests not only verified the effectiveness of the proposed inverse method, but also provided guidance to the practical experimental tests, such as the number and location of temperature sensors. It will produce better estimation if the sensors are located closer to the interface and more sensors are used. However, it is difficult to fix too many sensors or locate the sensors too close to the tool-chip interface due to the small region involved and the possible damage on the sensors by the chips. Based on the above numerical tests, the experimental cutting tests can be performed effectively and economically with 3–5 sensors with a distance about 4–8 mm.

5 Experimental tests

Experimental tests were performed to verify the thermal model and algorithms. A CNC lathe machine (GSK980TDb) was used to turn titanium alloy Ti-6Al-4V without any coolant. Figure 5a shows the whole experiment equipments and Fig. 5b shows a close view of the turning tool assembly, the cutting material, and the thermocouple installation details.

Table 3 The relative RMS error and time delay for different numerical tests

	Test no.	Test 1	Test 2	Test 3	Test 4	Test 5
Test conditions	Noise level (°C)	$\sigma = 5$ °C	$\sigma = 5$ °C	$\sigma = 5$ °C	$\sigma = 5$ °C	$\sigma = 10$ °C
	Number of sensors	3	2	1	3	3
	Average sensor distance	4 mm	4 mm	4 mm	8 mm	4 mm
Estimation errors (r): number of future measurement	Exact matching	15.2% (0)	36.7% (0)	42.8% (0)	68.6% (0)	46.3% (0)
	SFSM	3.1% (4)	7.5% (6)	8.1% (8)	9.2% (9)	8.5% (8)
	STRM	3.2% (0)	7.7% (0)	8.5% (0)	9.6% (0)	8.8% (0)

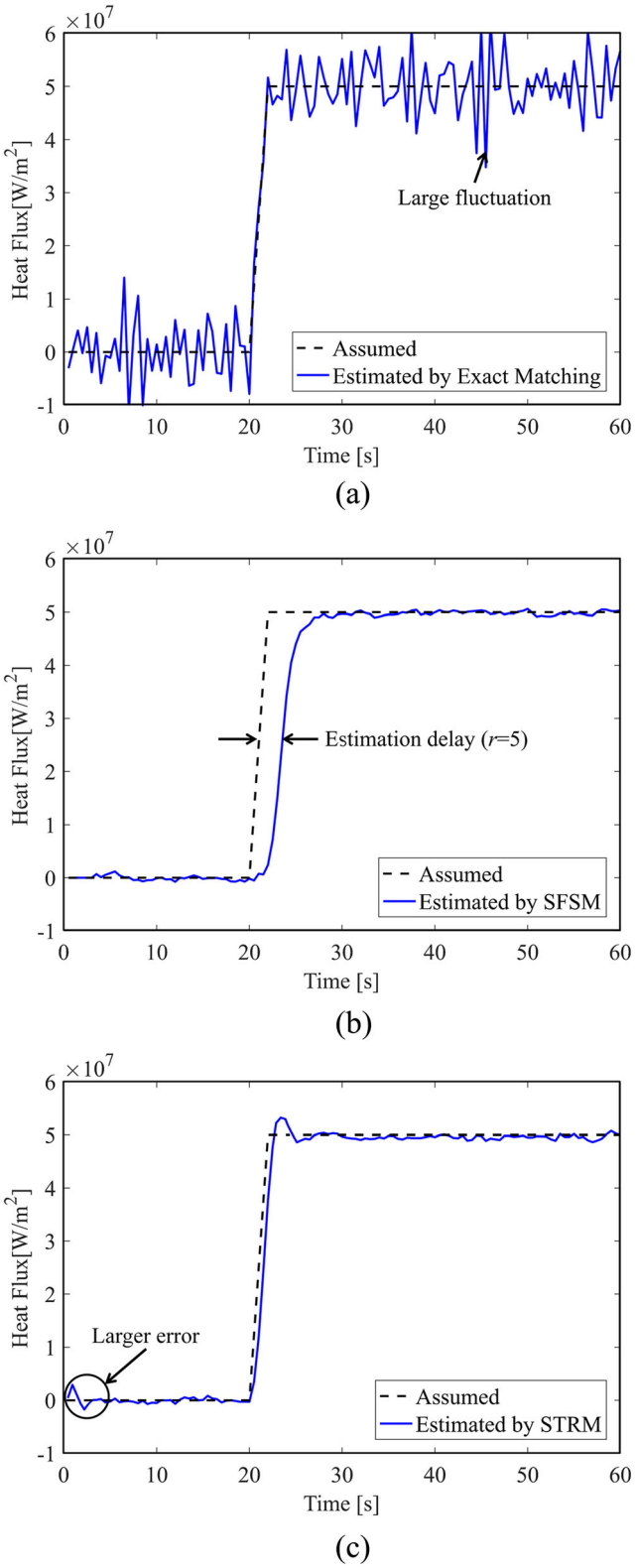

Fig. 4 Comparison between the assumed exact heat flux and the estimated heat flux of test 1 for **a** the exact matching method, **b** the SFSM with regularization parameter $r = 5$, and **c** the STRM with regularization parameters $\alpha = (3,100,10)$

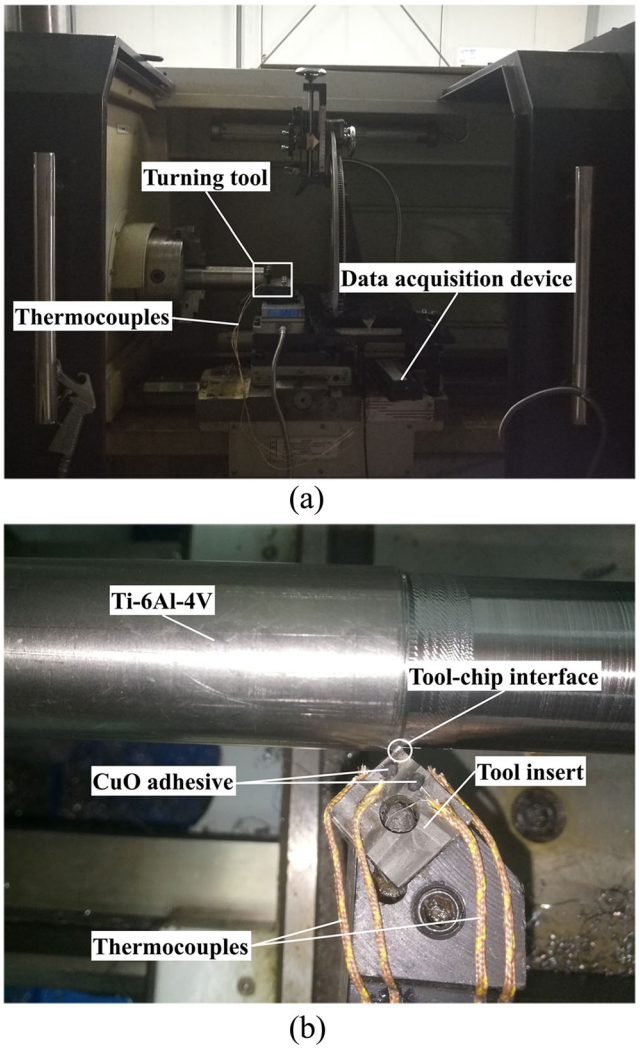

Fig. 5 Experiment setups. **a** The CNC lathe machine and other equipments. **b** A close view of the turning tool, cutting material, and thermocouple installation

Four K-type wire thermocouples (OMEGA, STC-GG-K-36), whose wire diameter is 0.13 mm, were fixed on the tool rake face by high temperature CuO adhesives and a data acquisition device (OMEGA, OMB-DAQ-54) was used to record the transient temperature measurements. The temperature measurements interval is 0.5 s, the same with the on-line procedure. Figure 6 shows the thermocouple locations at the turning tool and the model in ANSYS, respectively. Table 4 lists the exact coordinates of the thermocouples according to the Cartesian coordinate system.

The cutting parameters of two experimental tests, test 1 and test 2, are listed in Table 5. These two tests are with different feed rate and depth of cut and with the same cutting speed. The cutting speed is relatively small to avoid damage to the tool insert.

The time constant of thermocouple is defined as the time required to reach 63.2% of an instantaneous temperature change. This parameter is important for transient temperature

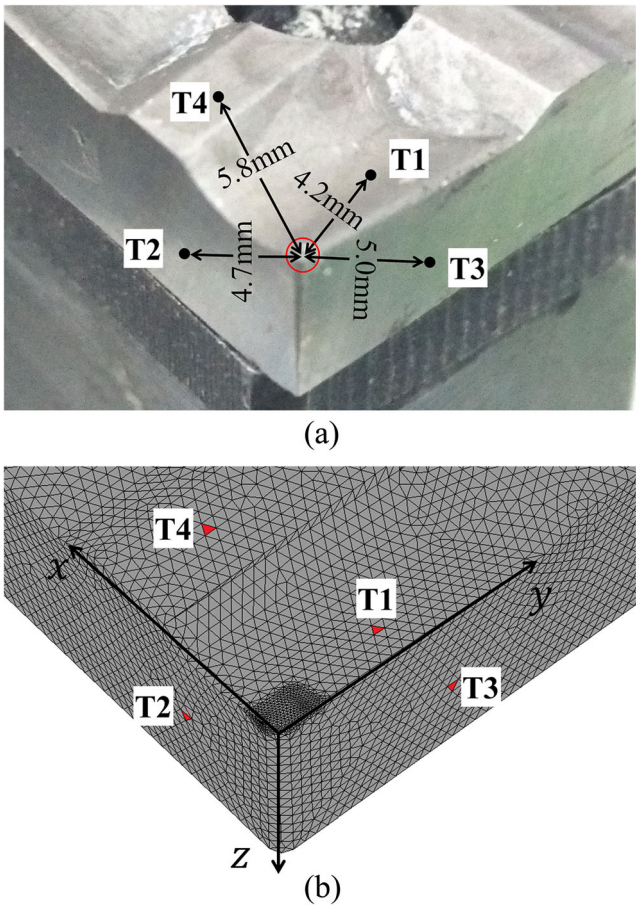

Fig. 6 The thermocouple installation location **a** on the practical turning tool and **b** on the meshed ANSYS model

measurement in machining, because cutting temperature rises rapidly at the transient cutting moment, while the thermal-inertial effect of thermocouple can lead to unavoidable measurement delay, which will inevitably result in delay and error in the heat flux and temperature field estimation. Therefore, the time constant of thermocouple used in on-line application should be as small as possible. Thus, thermocouples with small hot conjunctions are used in this study. The response time is about 0.1 s (found in OMEGA's official website), which is relatively small for a commercial thermocouple. The estimation delay caused by this thermocouple measurement is within 0.5 s.

The tool-chip interface area is one of the most important aspects among the main sources of errors in the solution of the

Table 4 Thermocouple location coordinates

Thermocouple no.	T1	T2	T3	T4
X [mm]	2.05	4.00	0	5.27
Y [mm]	3.65	0	4.38	2.48
Z [mm]	− 1.12	2.38	2.43	0

Table 5 Experimental cutting parameters

Cutting parameters	Test 1	Test 2
Cutting speed v_c [m/min]	30	30
Feed rate f [mm/rev]	0.2	0.1
Depth of cut a_p [mm]	0.8	1.0
Turning stage [s]	[20–152]	[10–85] [110–182]

thermal model. In this paper, this area was measured by a Shape Measurement Laser Microscope (Keyence, VK-X200K) and then treated by an image processing software (Keyence, VK Analyzer). The interface images of the two experimental tests are depicted in Fig. 7.

6 Results and discussions

An important task of the inverse procedure is to validate the accuracy of the thermal model. The best way is to compare

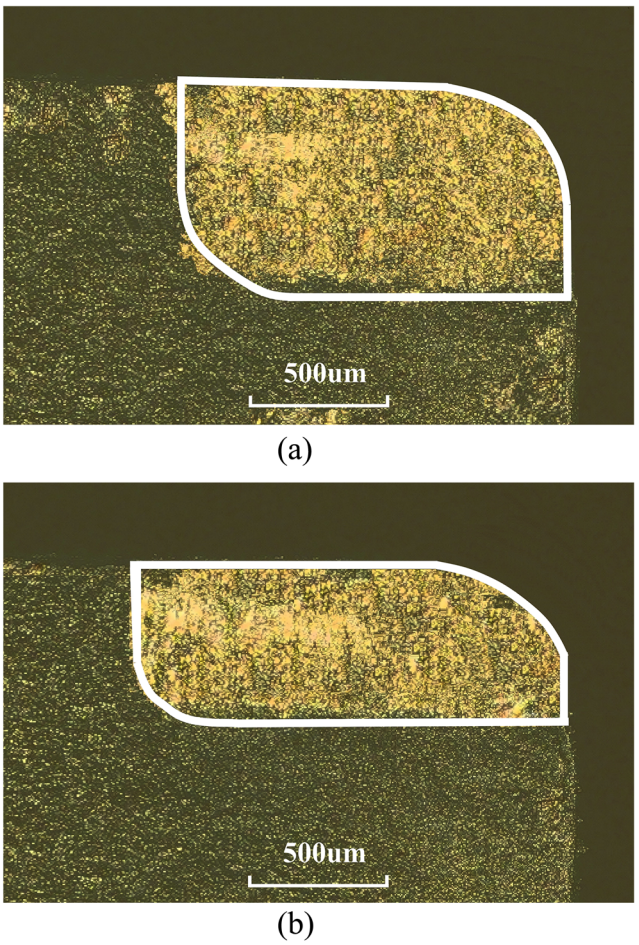

Fig. 7 Area of the tool-chip interface obtained by a video camera after the cutting process for **a** test 1 ($v_c = 30m/min, f = 0.2mm/rev, a_p = 0.8mm$) and **b** test 2 ($v_c = 30m/min, f = 0.1mm/rev, a_p = 1.0mm$)

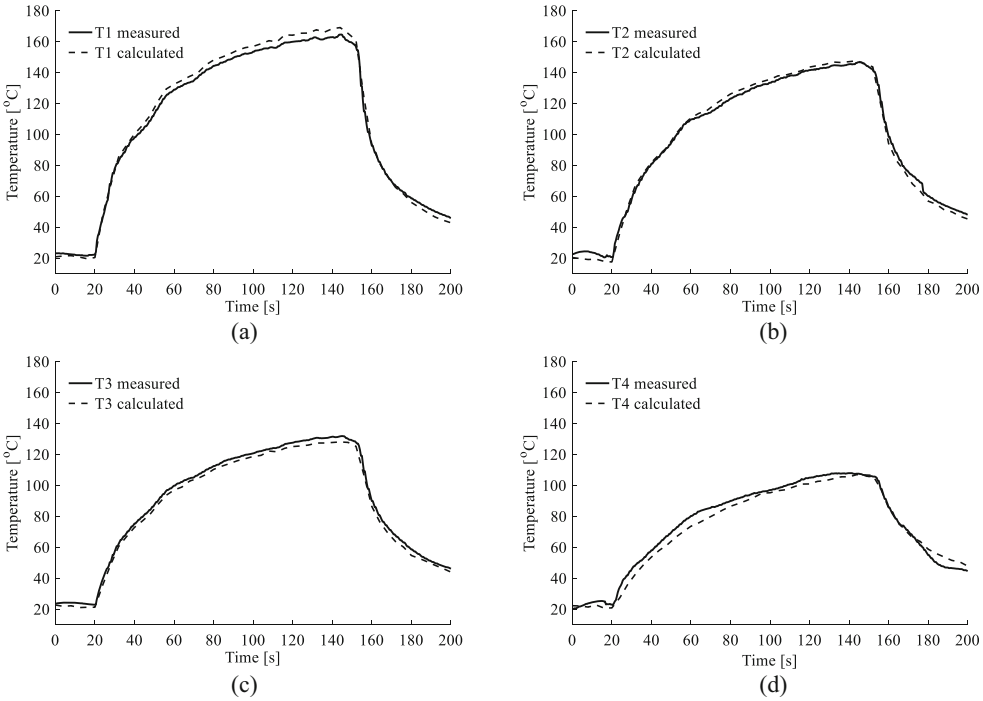

Fig. 8 The measured temperature and calculated temperature of sensor **a** T1, **b** T2, **c** T3, and **d** T4 for test 1

directly the estimated heat flux with the actual heat flux. However, as it is difficult to measure such quantity directly, an alternative and indirect approach is carried out. This was done by comparing the measured temperature of a single thermocouple with its calculated temperature, which was obtained by using the measurements of other three thermocouples as input to the procedure.

Figures 8 and 9 show the comparisons between the measured and calculated temperatures of all four thermocouples for test 1 and test 2, respectively. The estimation RMS errors are 2.78, 1.43, 2.18, and 3.85 °C for test 1; and 2.40, 1.13, 2.24, and 3.53 °C for test 2. The calculated and measured temperature curves are in good agreements. Although small deviation still exists, especially at the cutting-in and cutting-

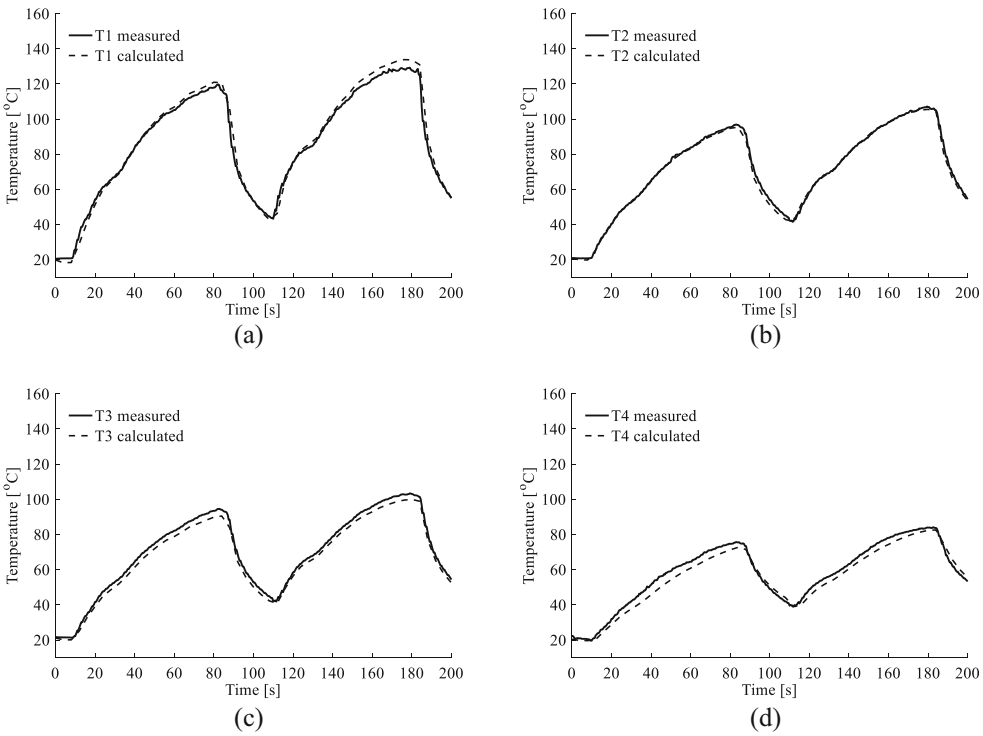

Fig. 9 The measured temperature and calculated temperature of sensor **a** T1, **b** T2, **c** T3, and **d** T4 for test 2

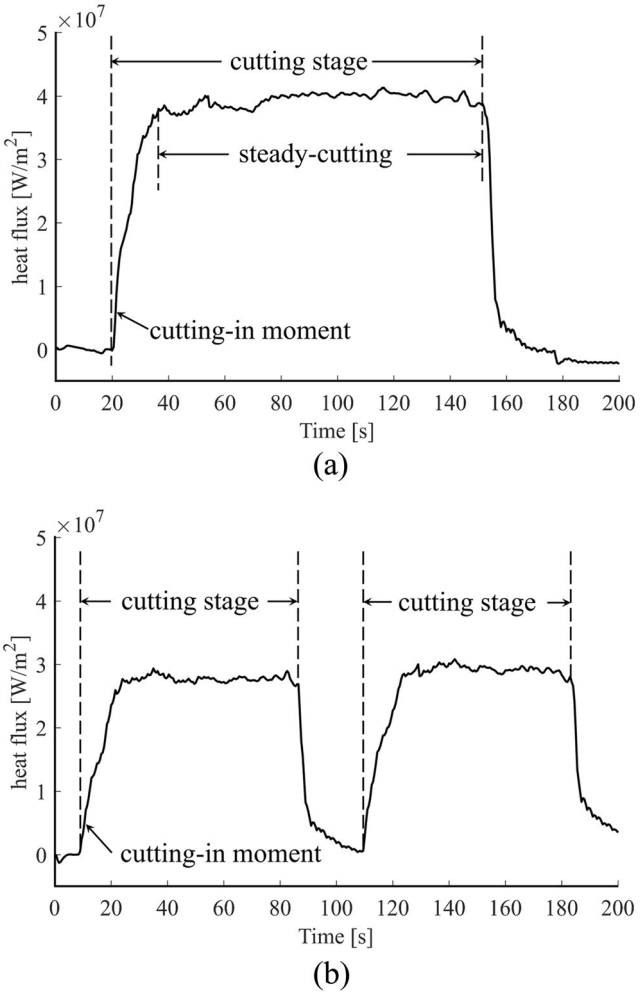

Fig. 10 The heat flux estimated by T1–T4 for **a** experimental test 1 and **b** experimental test 2

out moment when the heat flux changes most dramatically, however, the estimation errors are relatively small and within an acceptable range, as the relative RMS errors are all less than 2.5% of the maximum temperature. The accuracy of the thermal model is validated by these comparisons.

Figure 10 shows the estimated heat fluxes for test 1 and test 2. The estimated heat flux curves are smooth and match well with the actual cutting process. For instance, in Fig. 10a, the heat flux rises sharply at the beginning of the cutting (at 20 s), reaches a steady state after about 15 s of cutting, and goes to zero immediately when the cutting halts (at 152 s).

Unlike the thermocouple temperatures which keep rising during the whole cutting tests, the heat flux reaches a steady state rapidly, within just a few seconds. The difference is owing to the lag and damp effect of the heat transfer process, as the thermocouples are relatively far from the tool-chip interface.

Figures 11 and 12 show the reconstructed temperature field at the tool-chip interface at different cutting stages, namely, the cutting-in moment (0.5 and 1.0 s after cutting start) and the steady cutting stage ($t = 40$ s and $t = 120$ s for test 1 and $t = 60$ s and $t = 160$ s for test 2). Each of these figures was visualized using150 temperature points, which were calculated within 0.5 s.

Clearly, the maximum temperature is not exactly at the cutting edge but with a small distance, about 0.5 mm for test 1 and 0.3 mm for test 2. The temperature gradient is rather large in the tool-chip interface area, compared with the areas outside the interface, and the largest gradient is at the edge of the interface. Generally, the reconstructed temperature fields match quite well with the results reported in literature [27].

The tool-chip interface temperature rises rapidly at the cutting-in moment. For instance, in test 1, the maximum temperature rises from 21 to 346 °C in just 0.5 s and to 457 °C in 1.0 s; meanwhile, the temperature of thermocouple T4 only increases from 19.8 to 36.2 °C in 0.5 s and to 41.9 °C in 1.0 s. Similar result can be found in test 2. This indicates that the temperature rises more rapidly in the tool-chip interface than the outside regions. What is more, though estimation delay does exist because of the thermocouple's measurement delay, the dramatic changes of tool-chip interface temperature, especially at the cutting-in moment, can still be estimated by the method provided.

The temperature field reaches a relatively stable condition after several seconds of cutting, as can be seen in Fig. 11 that the temperature fields at $t = 40$ s and $t = 120$ s do not change much. This variation trend is similar to that of the heat flux, which responded rapidly to the changes of the cutting conditions.

Based on these data and figures, it is easy to obtain the average or maximum tool-chip interface temperature, to find the maximum temperature location, and to analyze the effects of cutting parameters on the temperature field variations.

7 Conclusions

In this paper, heat flux and temperature field at the tool-chip interface have been estimated in real time during the turning process, based on temperature measurements by several thermocouples located on the surface of the tool. A sequential inverse method as well as a combined method to solve the non-linear thermal model has been proposed. Numerical and experimental tests were carried out to verify the procedure's calculation efficiency, accuracy, and stability as well as the thermal model's accuracy. The main conclusions are as follows:

1. An inverse heat conduction problem (IHCP) of the turning tool is solved using a sequential Tikhonov regularization method (STRM). The proposed inverse method has a superiority in on-line application due to its sequential manner and independence of future measurement

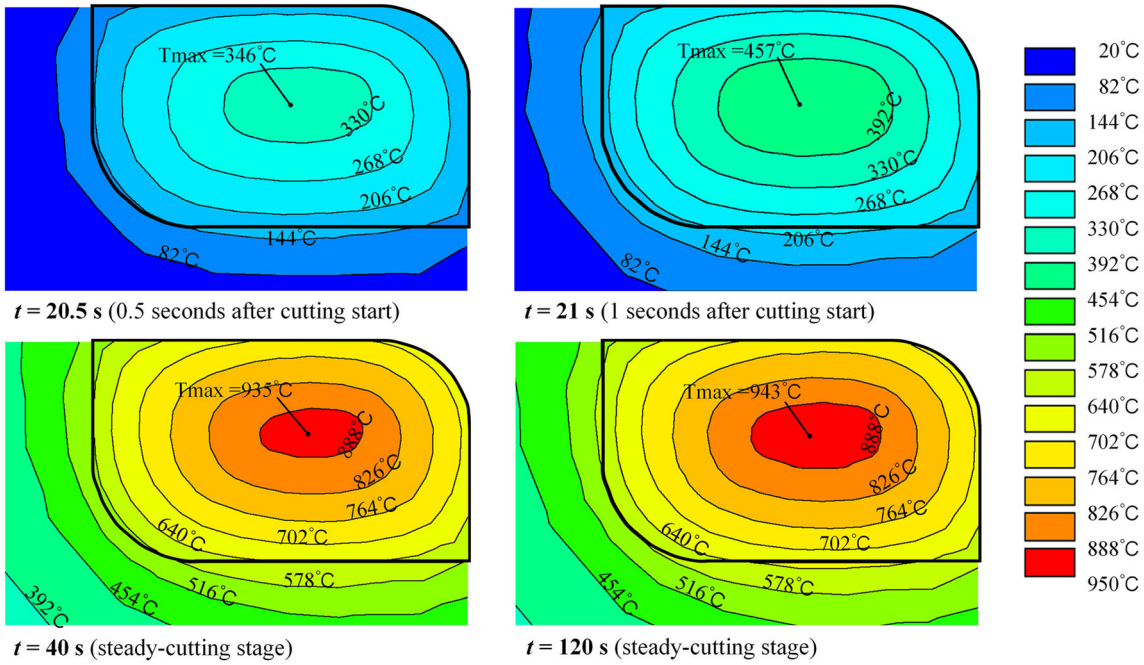

Fig. 11 Reconstructed temperature field of the tool-chip interface for experimental test 1

information. Such superiority has been verified by several numerical tests.

2. The non-linear thermal model of the tool is solved with high efficiency, combining Duhamel's theorem and the finite element method, and the accuracy of the thermal model has been verified by experimental cutting tests.
3. The heat flux and detailed temperature field at the tool-chip interface were estimated during turning process. The computation takes only 0.5 s at each time step, which enables the procedure to be applicable in on-line tool temperature monitoring.
4. Further researches can be conducted, such as the analysis of the turning mechanism and the effects of cutting conditions on tool temperatures, or the determination of heat partition coefficient during turning.
5. The proposed method is easy to implement in industry as only several thermocouples are required for temperature measurement. What is more, the procedure can be easily

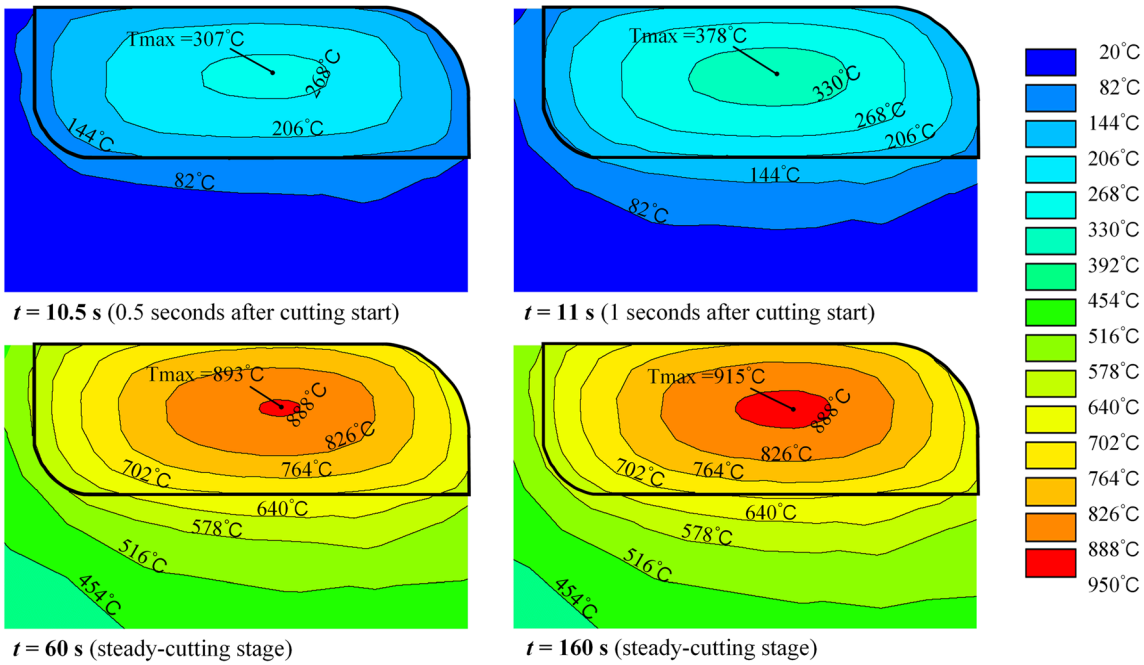

Fig. 12 Reconstructed temperature field of the tool-chip interface for experimental test 2

extended in the field of on-line heat source/heat flux identification or temperature field reconstruction in other machining or thermal processes.

Funding information The work is supported by the National Natural Science Foundation of China granted under No. 51575215 and U1501248 and the National Basic Research Program of China (973 Program) granted under No. 2013CB035803.

References

1. Jaspers SPFC, Dautzenberg JH, Taminiau DA (1998) Temperature measurement in orthogonal metal cutting. Int J Adv Manuf Technol 14(1):7–12
2. Le Coz G, Dudzinski D (2014) Temperature variation in the workpiece and in the cutting tool when dry milling Inconel 718. Int J Adv Manuf Technol 74(5–8):1133–1139
3. Grzesik W (1999) Experimental investigation of the cutting temperature when turning with coated indexable inserts. Int J Mach Tools Manuf 39:355–369
4. Kaminise AK, Guimarães G, da Silva MB (2014) Development of a tool-work thermocouple calibration system with physical compensation to study the influence of tool-holder material on cutting temperature in machining. Int J Adv Manuf Technol 73(5–8):735–747
5. Artozoul J, Lescalier C, Bomont O, Dudzinski D (2014) Extended infrared thermography applied to orthogonal cutting: mechanical and thermal aspects. Appl Thermal Eng 64(1–2):441–452
6. M'Saoubi R, Chandrasekaran H (2011) Experimental study and modelling of tool temperature distribution in orthogonal cutting of AISI 316L and AISI 3115 steels. Int J Adv Manuf Technol 56(9–12):865–877
7. Werschmoeller D, Li X, Ehmann K (2012) Measurement of transient tool-internal temperature fields during hard turning by insert-embedded thin film sensors. J Manuf Sci Eng 134(6):061004
8. Abukhshim NA, Mativenga PT, Sheikh MA (2006) Heat generation and temperature prediction in metal cutting: a review and implications for high speed machining. Int J Mach Tools Manuf 46(7–8):782–800
9. Loewen EG (1954) On the analysis of cutting-tool temperatures. Trans ASME 76:217
10. Zhang J, Liu Z, Du J (2017) Prediction of cutting temperature distributions on rake face of coated cutting tools. Int J Adv Manuf Technol 91(1–4):49–57
11. Li B, Li H, Liu J, Jia G (2017) An experimental and numerical investigation of temperature distribution on the ceramic cutting tool. Int J Adv Manuf Technol 92(9–12):4221–4230
12. Puls H, Klocke F, Veselovac D (2016) FEM-based prediction of heat partition in dry metal cutting of AISI 1045. Int J Adv Manuf Technol 86(1–4):737–745
13. Zhang Y, Gu Y, Chen JT (2010) Boundary element analysis of the thermal behaviour in thin-coated cutting tools. Eng Anal Bound Elem 34(9):775–784
14. Beck JV, Blcakwell B, Clair SR (1985) Inverse heat conduction problems: ill-posed problems. Wiley, New York
15. Yen DW, Wright PK (1986) A remote temperature sensing technique for estimating the cutting interface temperature distribution. J Eng Ind 108(4):252–263
16. Stephenson DA (1991) An inverse method for investigating deformation zone temperatures in metal cutting. J Eng Ind 113(2):129–136
17. Kwon P, Schiemann T, Kountanya R (2001) An inverse estimation scheme to measure steady-state tool-chip interface temperatures using an infrared camera. Int J Mach Tools Manuf 41:1015–1030
18. Lavisse B, Lefebvre A, Sinot O, Henrion E, Lemarié S, Tidu A (2017) Grinding heat flux distribution by an inverse heat transfer method with a foil/workpiece thermocouple under oil lubrication. Int J Adv Manuf Technol 92(5–8):2867–2880
19. Carvalho SR, Lima e Silva SMM, Machadoa AR, Guimar G (2006) Temperature determination at the chip-tool interface using an inverse thermal model considering the tool and tool holder. J Mater Process Technol 179:97–104
20. Huang CH, Lo HC (2005) A three-dimensional inverse problem in predicting the heat fluxes distribution in the cutting tools. Numer Heat TR A-Appl 48(10):1009–1034
21. Liang L, Quan YM, Ke ZY (2011) Investigation of tool-chip interface temperature in dry turning assisted by heat pipe cooling. Int J Adv Manuf Technol 54(1–4):35–43
22. Liang L, Xu H, Ke Z (2013) An improved three-dimensional inverse heat conduction procedure to determine the tool-chip interface temperature in dry turning. Int J Therm Sci 64:152–161
23. Wei B, Tan G, Yin N, Gao L, Li G (2016) Research on inverse problems of heat flux and simulation of transient temperature field in high-speed milling. Int J Adv Manuf Technol 84(9–12):2067–2078
24. Feng Y, Zheng L, Wang M, Wang B, Hou J, Yuan T (2015) Research on cutting temperature of work-piece in milling process based on WPSO. Int J Adv Manuf Technol 79(1–4):427–435
25. Norouzifard V, Hamedi M (2014) A three-dimensional heat conduction inverse procedure to investigate tool-chip thermal interaction in machining process. Int J Adv Manuf Technol 74(9–12):1637–1648
26. Brito RF, Carvalho SR, Lima e Silva SMM (2015) Experimental investigation of thermal aspects in a cutting tool using comsol and inverse problem. Appl Thermal Eng 86:60–68
27. Chen WC, Tsao CC, Liang PW (1997) Determination of temperature distributions on the rake face of cutting tools using a remote method. Int Comm Heat Mass Transfer 24(2):161–170
28. Samadi F, Kowsary F, Sarchami A (2012) Estimation of heat flux imposed on the rake face of a cutting tool: a nonlinear, complex geometry inverse heat conduction case study. Int Comm Heat Mass Transfer 39(2):298–303
29. Battaglia J-L, Kusiak A (2005) Estimation of heat fluxes during high-speed drilling. Int J Adv Manuf Technol 26(7–8):750–758
30. Mondelin A, Valiorgue F, Feulvarch E, Rech J, Coret M (2013) Calibration of the insert/tool holder thermal contact resistance in stationary 3D turning. Appl Thermal Eng 55(1–2):17–25
31. Woodbury K (2003) Inverse engineering handbook. Press, CRC